Intermetallics 91 (2017) 22–30

Contents lists available at ScienceDirect

Intermetallics

journal homepage: www.elsevier.com/locate/intermet

Exchange-bias reversal in $Mn_{2-x}Ni_{1+x}Ga$ films with antisite disorder

D.M. Schaefer[a,b,*], A.J.A. de Oliveira[c], P.C. de Camargo[c], J. Varalda[b], W.H. Schreiner[b], D.H. Mosca[b]

[a] Universidade Tecnológica Federal Paraná, Departamento de Física, 85884-000 Campus Medianeira, Parana, Brazil
[b] Universidade Federal do Paraná, Departamento de Física, 81531-980 Curitiba, Parana, Brazil
[c] Universidade Federal de São Carlos, Departamento de Física, 13565-905 Sao Carlos, SP, Brazil

ABSTRACT

We report on the exchange-bias reversal in $Mn_{2-x}Ni_{1+x}Ga$ (x = 0, 0.2, 0.4, and 0.6) thin films grown by molecular beam epitaxy on GaAs substrates. Exchange bias reversal is observed in these intrinsically ferrimagnetic films together with a reduction in the total moment even under increasing of Ni content which usually increases the total moment. These magnetic features indicate that antisite disorder is responsible for engender changes in the exchange-bias and total moment. Density functional theory calculations were performed to determine the magnetic moment dependence with the volume of cubic austenite and tetragonal martensite structures. A simple phenomenological approach is used to extract an effective exchange coupling constant from exchange bias fields.

1. Introduction

Among magnetic shape memory alloys (MSMA) the Ni-Mn-Ga alloys are widely studied due to exhibit martensitic transformations around room temperature with excellent shape memory behavior in single-crystal and polycrystalline samples [1–4]. The structural and magnetic properties of these stoichiometric (such as Ni_2MnGa and Mn_2NiGa) and off-stoichiometric alloys are relatively well established in bulk, but still little explored in the thin films, which geometry is crucial for actuators and sensing applications in macro- and nanodevices.

A crystal structure commonly adopted for stoichiometric X_2YZ alloys is the generalized Heusler-type structure, which is represented with four interpenetrating face-centered cubic sublattices, as shown in Fig. 1.

Depending on the crystallographic positioning of atoms on the four sublattices, different ordered structures can be obtained within a distinct space group (S.G.). A general composition is given by XXYZ structure which indicates X atoms occupying A and B sublattices, Y atoms occupying C sublattice, and Z atoms at D sublattices. Some alloys prefer to be formed with certain structures and others are never observed. Besides, chemically disordered alloys are ordinarily formed owing to the presence of antisite defects. It is a convention that X_X, X_Y or X_Z refers to an X atom at the X, Y or Z atomic site, respectively, whereas the distance between X atoms occupying A and C sublattices can be expressed as X(A)-X(C) [5].

Particularly, the ordered cubic Mn_2NiGa with lattice parameter a = 0.591 nm prefers the MnMnNiGa structure (S.G. 216) instead of the usual Heusler alloys with MnNiMnGa structure (S.G. 225). Therefore, interchanging tetrahedral Ni atom at (½, ½, ½) with octahedral Mn atom at (¼, ¼, ¼) and keeping the remaining atoms fixed at their positions. Mn atom at (0,0,0) are denoted as Mn_I and another one at (¼, ¼, ¼) as Mn_{II}. Disordered cubic structures tend to form a structure where Ga prefers the D sublattice, whereas Mn and Ni atoms prefer occupy their sublattices, but some Mn atoms occupy Ni sites and vice-versa [5–9].

Consistent theoretical studies of these alloys using density functional theory (DFT) are described at references [5–10]. Total moments between 1.18 μ_B/f.u. and 1.26 μ_B/f.u. are reported at room temperature for these ordered cubic structure with Mn magnetic moments at A sites antiparallel to the Mn moments at C sites, whereas total moments of about 2.13 μ_B/f.u. are obtained for disordered cubic structures. From this calculation results, Mn(A) moments between −2.27 μ_B and −2.56 μ_B, Mn(C) moments between +3.17 μ_B and +3.56 μ_B, and Ni moment of +0.35 μ_B are usually reported, depending on the computational approximations and other details. Anyway, for Mn_2NiGa there are two inequivalent Mn atoms at A and C sublattices whose moments are unequal and antiparallel depending on the presence of disorder, which lead to a ferrimagnetic ground state with small moment.

At low temperatures, the magnetic properties change through the martensitic transformation to a tetragonal structure (S. G. 139) with c/a ratio between 1.0 and 1.2 with a = 0.392–0.389 nm. Reduced total

* Corresponding author. Universidade Tecnológica Federal Paraná, Departamento de Física, 85884-000 Campus Medianeira, Parana, Brazil.
E-mail address: melloschaefer@gmail.com (D.M. Schaefer).

http://dx.doi.org/10.1016/j.intermet.2017.08.001
Received 17 March 2017; Received in revised form 30 July 2017; Accepted 1 August 2017
Available online 12 August 2017
0966-9795/

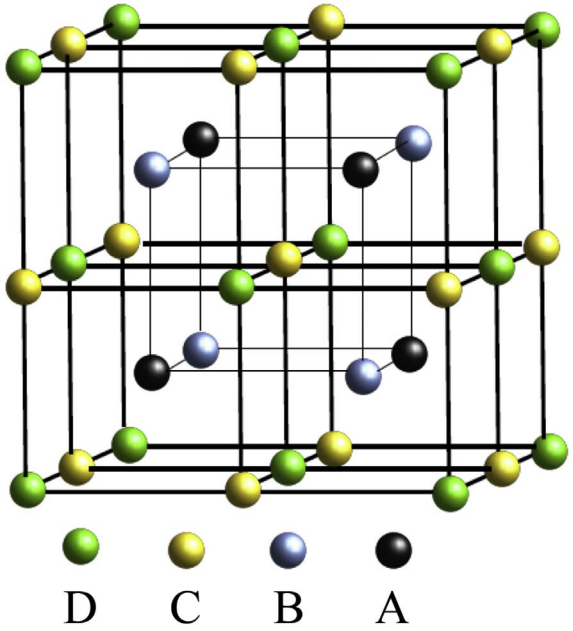

Fig. 1. The generalized Heusler-type structure with four interpenetrating fcc sublattices A(0,0,0), B(1/2,1/2,1/2), C(1/4,1/4,1/4), and D(3/4,3/4,3/4) used to describe cubic unit cells of the X_2YZ, where X, Y and Z are elements occupying each sublattice.

moments of about 1.12 μ_B/f.u. and 1.42 μ_B/f.u. are reported for ordered and disordered structures. The magnetic moment of Mn atoms decrease upon martensitic transformation to a tetragonal structure. Essentially, the large Mn-Mn distances difference in MnNiMnGa (0.295 nm) and MnMnNiGa (0.256 nm) implies significantly different magnetic properties in these two types of structures.

Although the interatomic magnetic interactions *per se* are complicated, it is commonly accepted that the magnetic ordering in ordered Mn-rich alloys seems to be only a function of the nearest Mn-Mn distance [6,7,11,12]. The smaller separation between Mn atoms in MnMnNiGa gives rise to parallel alignment between Mn(A) and Mn(B) magnetic moments, whereas large separation among Mn atoms, which is the case in MnNiMnGa structure and within each sublattice of Mn(A) and Mn(C), lead to whether parallel or antiparallel alignments between Mn atoms.

Additionally, both single-crystal and polycrystalline Mn_2NiGa alloys always have some degree of chemical disorder owing to the presence of antisite disorder, where some of the Ni or Ga sites are occupied by Mn atoms and vice-versa. Neutron diffraction experiments were used to the determination of the actual atomic occupancies and the degree of disorder [10,13]. These experiments revealed that the Mn atoms occupying Ni and Ga sites (Mn_{Ni} and Mn_{Ga}) cause the formation of ferromagnetic (FM) nanoclusters with parallel alignment of Mn spin moments in a Mn_2NiGa bulk lattice that has two sublattices with antiparallel Mn spin moments [13].Antisite disorder reaching more than 10% of the Ga sites occupied by Mn atoms in FM nanoclusters were reported. Apparently, such behavior might be typical of alloys with stoichiometry close to Mn_2NiGa. The local magnetic moments reported for Ni, Mn_{Ni}, Mn_{Mn}, and Mn_{Ga} are 0.40, −2.39, 3.34, and 3.41 μ_B, respectively. The antiferromagnetic (AFM) interaction between Mn_{Ga} and Mn_{Mn}, which are nearest neighbors 0.258 nm apart, results from the exchange pair interaction at relatively short Mn-Mn distance [11]. On the other hand, Mn_{Ga} atoms located on the next nearest neighbor of Mn_{Mn} at a separation of 0.277 nm exhibit ferromagnetic interaction [12]. Therefore, cluster moments randomly distributed in the samples containing Mn_{Ga}-Mn_{Mn} and Mn_{Ni}-Mn_{Mn} magnetically coupled pairs arise from the antisite disorder.

In a previous work, we focused on the study of the structure and magnetic properties of Mn_2NiGa thin films grown on GaAs substrates [14]. A small magnetic field induced reorientation effect is observed in these thin films in the absence of applied stress. In this paper, we will focus on off-stoichiometric $Mn_{2-x}Ni_{1+x}Ga$ films grown in the same way those in the previous work and study their magnetic properties. These films exhibit a predominant cubic structure at room temperature with a high crystalline texture in which (110) planes are aligned parallel to the film surface with lattice parameters a in the range between 0.589 nm and 0.574 nm. Saturation magnetization values are comprised between 1.23 μ_B/f.u. and 0.54 μ_B/f.u. at room temperature. These films exhibit narrow magnetic hysteresis loops at room temperature, but their hysteretic loops greatly open by decreasing the temperature. Furthermore, shifts of the hysteresis loops away from zero-field are observed as a function of the temperature, indicating the manifestation of exchange bias phenomena. More surprisingly, we describe and discuss an intrinsic exchange-bias reversal in single-phase ferrimagnetic alloys which is dependent on the stoichiometry of the films.

2. Experimental

The experiments were performed in a custom-designed ultrahigh vacuum multi-chamber system equipped with Mn, Ni, and Ga effusion cells. The Mn-Ni-Ga alloy films were simultaneously grown by molecular beam epitaxy (MBE) technique on (001)- and (111)-oriented GaAs substrates. Before the growth of the films, the oxide layers of the epi-ready GaAs wafers were removed by thermal desorption with simple heating at 520 °C for 10 min [15]. The clean wafer surfaces were monitored with *in situ* reflection high energy electron diffraction (RHEED) analyses. After thermal oxides desorption, (111)B-(1 × 1)- and (001)B(1 × 1)-reconstructed surfaces were stabilized. The growth procedures were then performed keeping the substrate temperatures at 200 °C. Alloys thin films with atomic proportion Mn:Ni:Ga given by (2 − x): (1 + x): 1 with x = 0, 0.2, 0.4, and 0.6 were prepared on the substrates by opening Mn, Ni, and Ga shutters during 30 min. Appropriated proportional fluxes of these elements were previously calibrated by using X-ray Photoelectron Spectroscopy (ESCA VG Microtech 3000) system which is *in tandem* with MBE chamber. XPS analyses were performed using an electron spectrometer equipped with a conventional Mg X-ray source and a 250 mm hemispherical energy analyzer with an overall resolution of 0.8 eV at a 45° emission angle. During growth procedures, Ni and Ga cell temperatures were respectively fixed at 1370 °C and 715 °C, whereas Mn cell temperature was kept at 835, 825, 815, and 810 °C to control the alloying x = 0, 5, 10, and 16 in the films. The determination of elemental composition have uncertainties lower than 3 at. % and as-deposited films have no evidence of carbon or oxygen contamination. Immediately after depositions, all films were annealed at 470 K during 2 h. Such annealing procedure does not promote significant change in the surface stoichiometry, but chemical ordering effects cannot be discarded [16]. At the end of the annealing procedure, the sample-holder temperature with samples is lowered to room temperature. All films are shiny with metallic appearance. RHEED patterns from GaAs surfaces are progressively faded away in the first 10 min of growth and only patterns consisting of streaks are observed after depositions. The annealing procedure only reduces the diffuse background making the streaks more visible in the RHEED patterns.

X-ray diffraction (XRD) measurements were performed at room temperature using Cu-Kα radiation. The experiments were done in Bragg-Brentano geometry with θ-2θ scan using Shimadzu XRD7000 and Bruker D8 Advanced equipments. The film thicknesses are 84 nm according to previous calibration using X-ray reflectivity experiments. The magnetic properties were characterized using vibrating sample magnetometers attached to Physical Property Measurement Systems (PPMS Evercool II and MPMS3 from Quantum Design). In all magnetic measurements, the applied magnetic fields were always applied parallel to the plane of the film. The magnetic hysteresis loops were recorded under zero-field cooling protocol, exhibit exchange bias effect which have been demonstrated to be characteristic of ferrimagnetic order. In

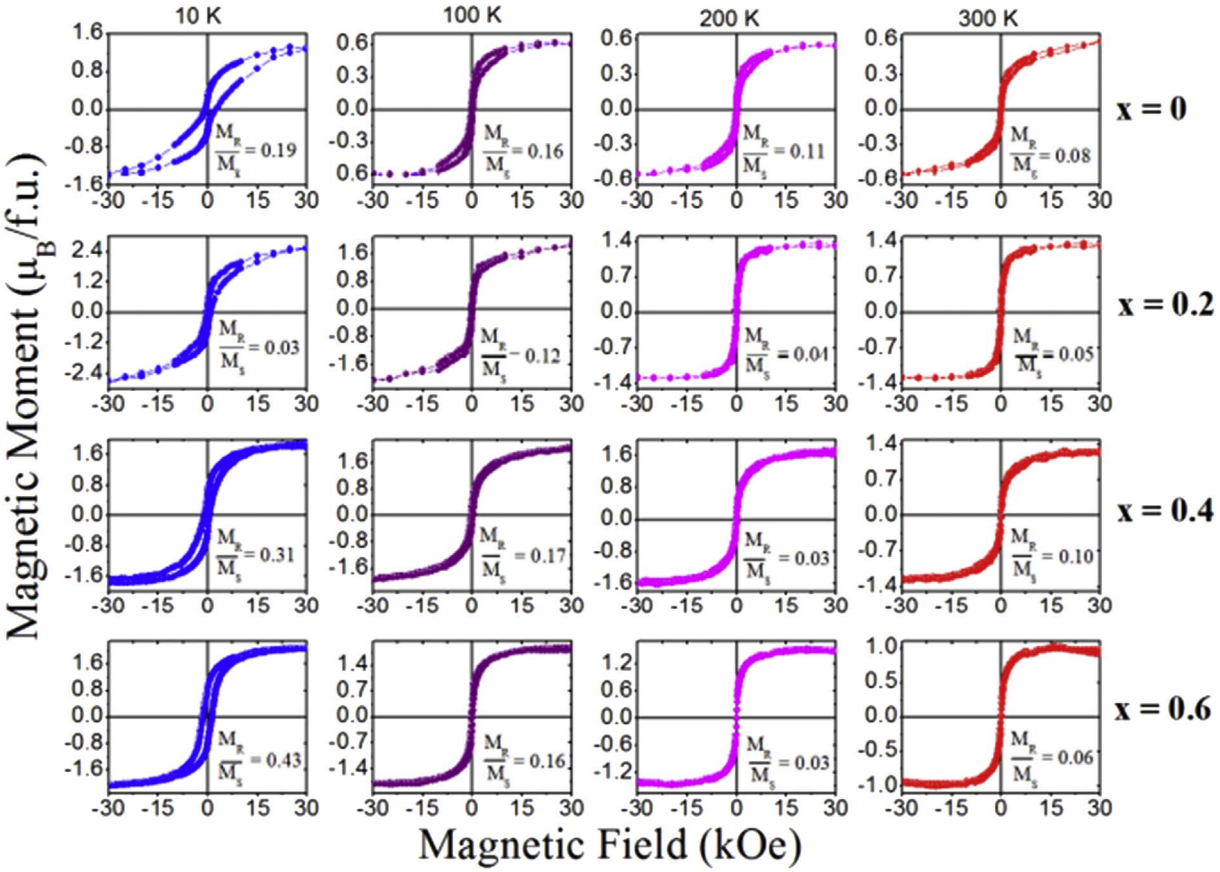

Fig. 2. Hysteresis loops measured at different temperatures for $Mn_{2-x}Ni_{1+x}Ga$ (x = 0, 0.2, 0.4, and 0.6) thin films grown on GaAs substrates with magnetic field applied in the film plane.

Table 1
Identification of $Mn_{2-x}Ni_{1+x}Ga$ films by alloying stoichiometric proportion (x) and cubic *a* lattice parameter. Saturation magnetization M_S, coercive field $H_C = (H_R - H_L)/2$, and exchange bias field $H_{EB} = (H_R + H_L)/2$ values, defined by $H_{R,L}$ corresponding to switching fields at positive and negative applied fields. The field offset error due to the effect of magnet remanence in the superconducting solenoid at low fields was subtracted from the values of H_C and H_{EB}. The values of H_{EB} above 100 K were set to zero because they are similar to the offset error.

Ratio x	Lattice *a* (nm)	M_S (μ_B/f.u.)				H_C (Oe)				H_{EB} (Oe)			
		10 K	100 K	200 K	300 K	10 K	100 K	200 K	300 K	10 K	100 K	200 K	300 K
0	0.5849	1.32	0.62	0.55	0.54	1540	140	110	125	+820	0	0	0
0.2	0.5855	2.28	1.55	1.28	1.23	495	190	5	5	+245	0	0	0
0.4	0.5982	1.79	1.64	1.43	1.08	785	275	130	100	−245	0	0	0
0.6	0.5826	2.05	1.8	1.4	0.92	1390	130	30	60	−80	0	0	0

the experiments performed with field linearly decreasing from 50 kOe to zero, the effect of magnet remanence in the superconducting solenoid at low fields leads to an offset error in the reported magnetic field which ranged in between 20 Oe and 37 Oe.

3. Results and discussion

3.1. Hysteresis loops

Magnetic measurements of the hysteresis loops shown in Fig. 2 were performed immediately after to increase the sample temperature up to 400 K to mitigate the magnetic memory effects.

At 300 K, the saturation magnetization (M_S) for off-stoichiometric $Mn_{2-x}Ni_{1+x}Ga_1$ films is found between 1.23 μ_B/f.u. and 0.54 μ_B/f.u., whereas M_S values at 10 K are ranged in between 2.05 μ_B/f.u. and 1.32 μ_B/f.u. In these alloys, the M_S values are somewhat controversial in the literature due to their dependence with the lattice parameters and antisite disorder [13,17].

The magnetic loops recorded at $T \leq 300$ K exhibit finite coercivity and low remanent magnetization indicating a build up of ferrimagnetic interactions which are inherent of this system. Such behavior can also be associated with ferromagnetic domains ascribed to antisite disorder [13]. Coercivity values depend on the alloy stoichiometry and increases with decreasing temperature below 200 K. At 10 K, the coercivity of the sample set range between 515 Oe and 1560 Oe.

A remarkable feature of these films is the presence of intriguing field shifts away from zero in the magnetic hysteresis loops as a function of the temperature. This feature is a characteristic of the so-called exchange bias effect [18], which is caused by spins coupled between ferromagnet/antiferromagnet (F/AF) interfaces that usually results in a field shift of the hysteresis loop away from zero and an enhanced coercivity when the system is field cooled (FC) through the Néel temperature (T_N) of the AF. At 10 K, substantial values of positive and negative exchange-bias fields are found as shown in Table 1. At 300 K, the parent cubic austenite structure show much smaller exchange bias fields.

The saturation magnetization tends to increase with decreasing temperatures, leading to martensites with higher total magnetic

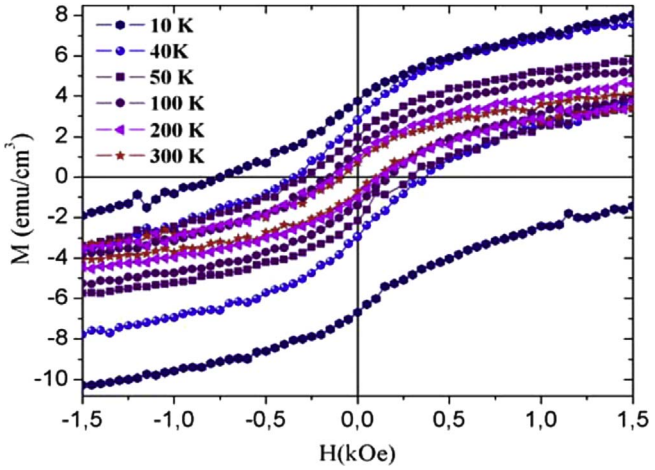

Fig. 3. Inner part of magnetic hysteresis loops measured at different temperatures with magnetic field applied in film plane of $Mn_{2-x}Ni_{1+x}Ga$ film with x = 0.

Table 2
Shorter and longer distances of nearest-neighbor inter-sublattice Mn_{Mn}-Mn_{Ni} sites normalized by the lattice parameter in austenite and martensite Mn_2NiGa structures.

Structure	Mn_{Mn}-Mn_{Ni} distance (nm)	R_{ij}/a ratio
A1	0.263	0.432
A3	0.248	0.433
M1	0.271	0.464
M6	0.250	0.462

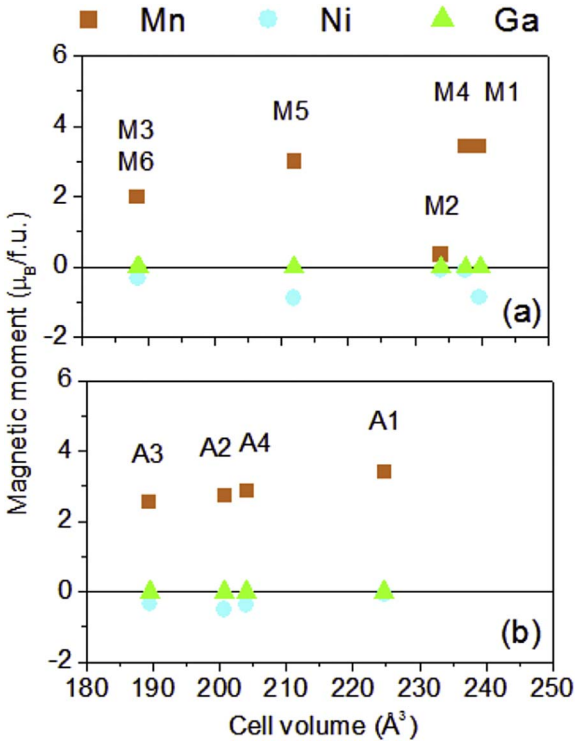

Fig. 4. Magnetic moments on atomic sites of Mn_2NiGa resulting from DFT calculations for: (a) martensite (M) and (b) austenite (A) structures identified as: M1 (a_1 = 0.5846 nm and c_1 = 0.7016 nm), M2 (a_2 = 0.5798 nm and c_2 = 0.6958 nm), M3 (a_3 = 0.5394 nm and c_3 = 0.6473 nm), M4 (a_4 = 0.5840 nm and c_4 = 0.6967 nm), M5 (a_5 = 0.5624 nm and c_5 = 0.6698 nm), A1 (a_1 = 6080 nm), A2 (a_2 = 0.5855 nm), A3 (a_3 = 0.5743 nm), and A4 (a_4 = 0.5887 nm). These nomenclatures for structures will be hereafter used in this work.

moment than austenites. The variation of the total magnetic moment of $Mn_{2-x}Ni_{1+x}Ga$ as a function of x from x = 0 to 1; i.e., decreasing Mn concentration from Mn_2NiGa to Ni_2MnGa, shows a trend for increasing in the austenite and martensite structures. Such increase is explained through a linear increase of Mn_{Mn} moment concomitant with faster increase of Mn_{Ni} moment that is colinear and opposite [7]. In our films, M_S values does not show a monotonous increase with the content of Ni in the alloy, indicating an effect of antisite disorder. Unfortunately, the crystalline texture of the thin films grown on GaAs substrates makes it difficult to access the Bragg reflections necessary for an adequate quantification of the antisite disorder by the proportion of the diffracted intensities normalized by their respective structure factors.

The inner part of some magnetic hysteresis loops of a stoichiometric Mn_2NiGa exhibiting reverse exchange bias (positive field-shift away from zero) as a function of temperature are shown in Fig. 3. According to Table 1, the exchange bias field changes from positive to negative in Mn-rich alloys with similar lattice parameters by increasing Ni content. The H_{EB} normally is negative reflecting the equilibrium spin configuration (FM moment is aligned along external field H). H_{EB} becomes positive in a metastable state with FM moment pointing to the direction opposite to the applied field. A metastable state is found to exist within a short field range before magnetization reversal. A first assumption for exchange bias origin owing to Mn-rich regions in the films and their possible oxidation in contact with air. However, it can be easily discarded since no evidence of Mn oxides are found from XRD data. Indeed, the exchange bias observed in these films have their magnitude and sign depending on the alloy composition and temperature, as shown in Table 2. Despite exchange bias has been already reported for Mn_2NiGa [14] straightforwardly related to the antisite disorder realized through neutron diffraction experiments [13], positive exchange bias field H_{EB}; i.e., H_{EB} shift is in the same direction as cooling field, is a quite unusual phenomena involving ferrimagnet/ferromagnetic interfaces [19,20].

3.2. DFT calculations

In order to better understand the electronic and magnetic structures of our thin films, we describe the electronic charge densities and magnetic moment distributions determined using DFT calculations performed for ordered Mn_2NiGa with MnMnNiGa structures with lattice parameters consistent with our films. Density functional theory calculations were performed using ELK all-electron full-potential linearized augmented-planewave (FP-LAPW) method implemented in ELK [21] code for determining the properties of crystalline ordered Mn_2NiGa alloys with inverse-type Heusler structure. We used GGA exchange correlation functional within the PBEsol approximation [22] for the non-collinear spin-polarized calculations. A grid of 8 × 8 × 8 k points in the Brillouin zone was used for the integration in reciprocal space. The total energy and the Kohn-Sham potential convergences were better than 10^{-5} Ha and 10^{-7} Ha, respectively. Some figures shown below were made using VESTA software [23].

Our *ab initio* calculations were performed for cubic Mn_2NiGa structures (S.G. 119) having lattices parameters a between 0.539 nm and 585 nm as well as tetragonal Mn_2NiGa structures (S.G. 119) with c/a ratio arbitrarily fixed at 1.2 and c values between 0.702 nm and 0.645 nm. The lattice parameters for the cubic structures were determined from the (220) Bragg reflection peaks obtained from X-ray diffraction measurements performed at room temperature. The choice to hold c/a = 1.2 for the tetragonal structures was based on similarity of the crystalline texture of the off-stoichiometric films with stoichiometric Mn_2NiGa (x = 0) films, which were previously investigated using X-ray diffraction technique in the temperature interval between 83 K and 473 K [14].

Our calculations reproduced quite well the electronic band structure and density of states previously reported by many theoretical works. Here, it is explored the magnetic moment dependence on the lattice

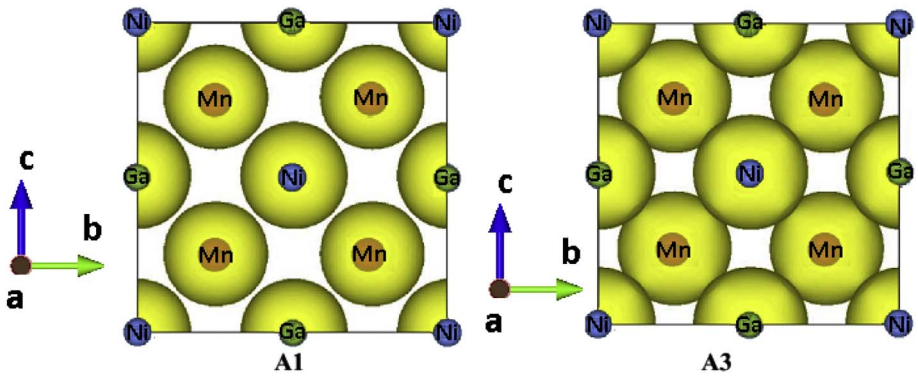

Fig. 5. Equivalent isosurfaces of the electronic charge densities corresponding to A1 and A3 austenite structures with lattice parameters a = 0.608 nm and 0.589 nm, respectively.

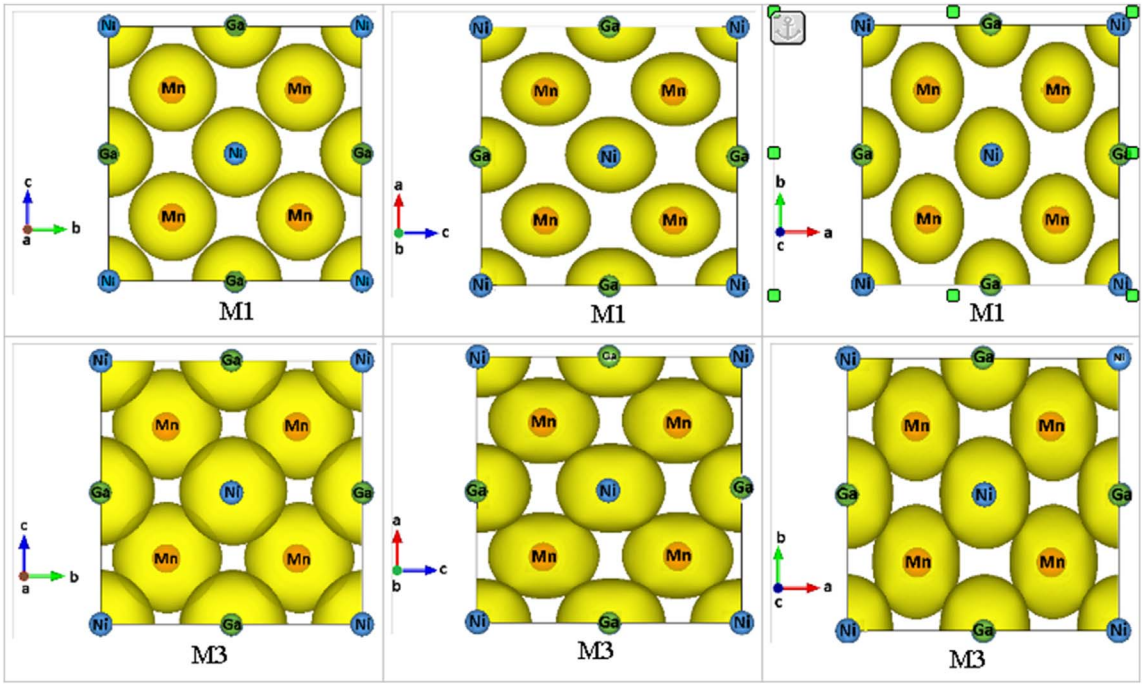

Fig. 6. Equivalent isosurfaces of electronic charge densities with two-dimensional projections along the three crystallographic axes for M1 and M3 martensite structures.

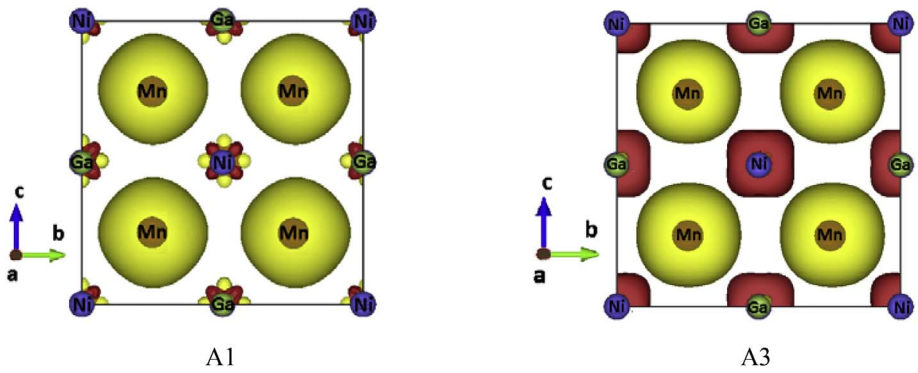

Fig. 7. Equivalent isosurfaces of magnetic moment distributions in A1 and A3 austenite structures. Opposite orientations of the magnetic moments around the atomic sites are colored in yellow and red.(For interpretation of the references to colour in this figure legend, the reader is referred to the web version of this article.)

parameters observed in our thin films. In Fig. 4(a) and (b) are shown the elemental magnetic moments as expected for austenitic and martensitic unit cells, respectively.

Rigorously, a ferrimagnetic ordering is expected for these alloys either at cubic or tetragonal cells, as shown by Fig. 4(a) and (b). It is worth noticing that the calculated total moment for stoichiometric ordered films (approximately 1.73 μ_B/f.u. for A1 and M1 structures) are much higher than experimental values found at for $x = 0$, as shown in Fig. 2. These theoretical results strongly indicate that chemical disorder certainly is occurring in these alloy thin films and possibly lead to a reduction in the total moment per unit cell. Additionally, the first nearest-neighbors inter-sublattices Mn_{Mn}-Mn_{Ni} interactions separated with distances R_{ij} can exhibit an AFM exchange parameter J_{ij} for R_{ij} smaller than lattice parameter a; *i.e.*, the Mn atom in Ni position becomes antiferromagnetically aligned to the original Mn atom and the total magnetic moment per cell decreases [7]. Typically, the AFM interaction occurs for $R_{ij}/a < 0.8$ and the reason for the opposite alignment is a direct Mn-Mn interaction, whereas magnetic Mn_{Ni}–Ni

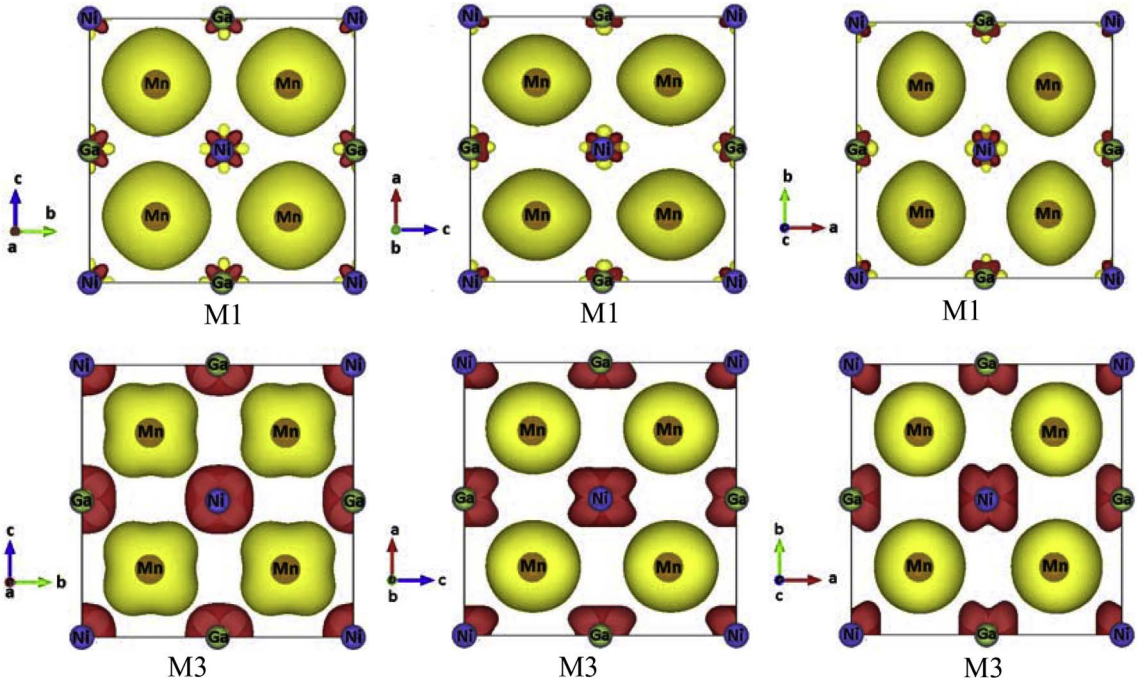

Fig. 8. Equivalent isosurfaces of magnetic moment distributions along the three crystallographic axes of M1 and M3 martensitic structures. Again, opposite orientations of the magnetic moments observed in the two-dimensional projections are colored in yellow and red.(For interpretation of the references to colour in this figure legend, the reader is referred to the web version of this article.)

interaction is much weaker in the first nearest-neighbors. Table 2 gives R_{ij}/a ratios for Mn_{Mn}–Mn_{Ni} in our stoichiometric films. As can be seen, R_{ij}/a ratios are between 0.46 and 0.43 in our structures favoring antiferromagnetic Mn_{Mn}–Mn_{Ni} interactions. Such AFM interactions can even dominate in the sample regions with stronger antisite disordering creating compensated AFM interfaces relatively to non-disturbed regions.

The isosurfaces of the electronic charge densities for two austenite structures are shown in Fig. 5. Both exhibit isotropic electronic charge densities along the crystallographic axes, whatever are the lattice parameter values. Clearly, smaller is the lattice parameter densest is the charge distribution within the two-dimensional projected unit cells.

Martensite structures with distinct lattice parameters (c/a = 1.2) exhibit equivalent isosurfaces of charge densities with tetragonally-distorted symmetry, as shown in Fig. 6.

Again, smaller is the lattice parameters densest are the electronic charge distributions within their respective unit cells and more tetragonally distorted becomes the electronic clouds.

Let us now address the magnetic moment distribution around the atomic sites. Some insight about cell dimensional effect on the magnetic behavior of Mn_2NiGa with MnMnNiGa structures are given through Figs. 7 and 8 where are shown main two-dimensional projections of the magnetic moment distributions in the austenite and martensite structures, respectively.

Clearly, the Mn moments are mostly isotropic distributed along the crystallographic axes and they remain parallel to each other whatever is the lattice parameters of the austenite structures. In contrast, Ni moments are anisotropically distributed along the crystallographic axes. By increasing the lattice parameter from A3 to A1 structure, Ni moments become more opposed to the Mn moments with an elongated delocalization along the [110] crystallographic directions, which implies in some degree of magnetic anisotropy.

Tetragonal symmetry of the martensitic structures also affect the magnetic moment configurations, as can be seen from the two-dimensional projections shown in Fig. 8.

For Mn sublattice, the magnetic moments remain parallel to each other whatever is the lattice parameters investigated in this work. Some weak uniaxial magnetic anisotropy is expected for matersite structure M1, whereas a biaxial magnetic anisotropy along the [110] crystallographic directions is expected for M3. In regard to Ni moment distribution some magnetic anisotropy is expected in M3, comparatively to M1 due to asymmetry along the [110] crystalline axes. Our calculations, however, suggest small magnetic anisotropies in both austenite and martensite structures, as observed in our thin films whatever is the orientation of the GaAs substrate.

To evaluate the magnetization changes induced by antisite disorder involving Mn occupying Ni sites and vice versa, first-principles DFT calculations were also performed for Mn_2NiGa (x = 0) having martensitic M3 structure. According to our calculations, the magnetic moment configurations leading to total energy minimization in each structure correspond to fundamental electronic structure consistent with ferrimagnetic states. The configuration of the magnetic moments along the (001) crystalline planes of ordered and disordered martensite structures are shown in Fig. 9.

In the case of the ordered martensitic structure shown in Fig. 9(a), the magnetic moments of equivalent Mn sites tend to remain collinear and parallel to each other. The same configuration of magnetic moments is found in equivalent Ni sites. However, the magnetic moments of Ni are about one order of magnitude smaller than the moments of Mn. The sublattices of Mn and Ni are collinear, but their magnetic moments are opposed.

The introduction of chemical disorder with Mn atoms occupying preference sites of Ni and vice versa, the configuration of magnetic moments drastically changes, as we can see in Fig. 9(b). The magnetic moments of Mn and Ni atoms contained in plane (001) become collinear and parallel to each other although they have distinct magnitudes. Differently, the magnetic moments of Mn and Ni contained in the plane ($00^1/_4$) turn back to have distinct magnitudes although they remain collinear and parallel. Since the magnetic moments of these two atomic planes are collinear and opposite, the total magnetic moment of the disordered structure decreases.

The spin configurations of martensite structure containing disorder with Mn atmos occupying (¾. ¾, ¾) and (½, ½. ½) sites (often referred to MnI and MnII) are similar, except that magnetic moment magnitudes

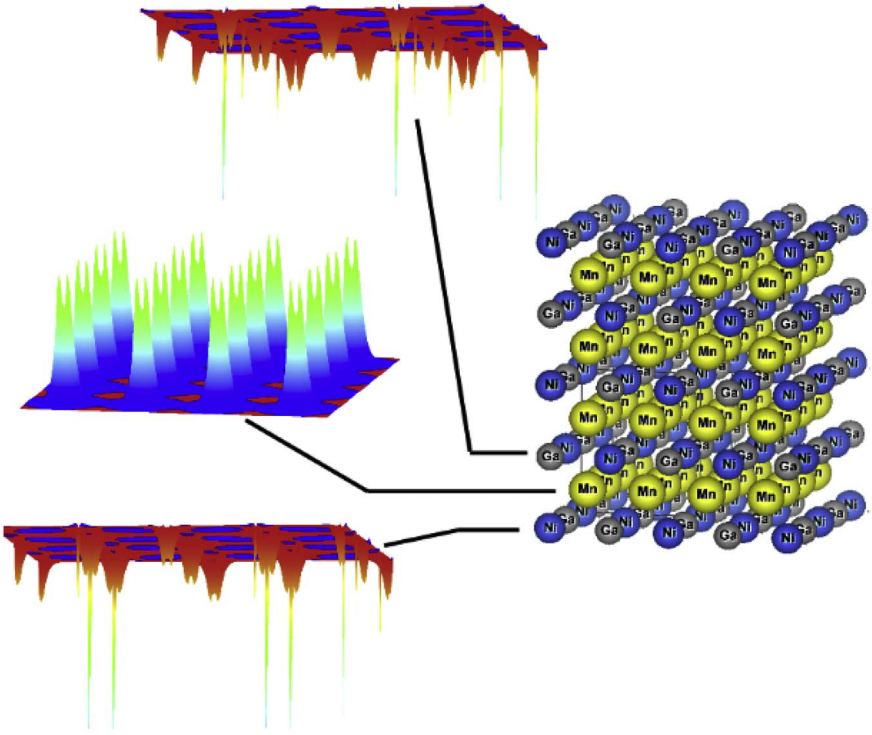

(a)

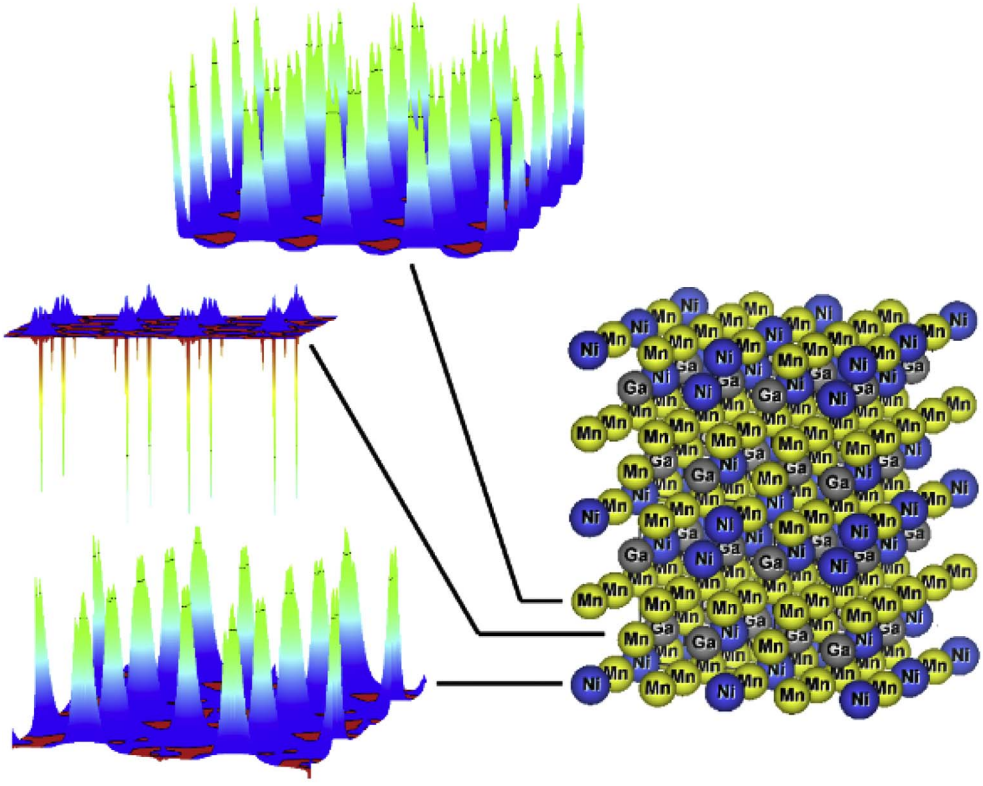

(b)

Fig. 9. Three-dimensional plot of the spin magnetic-moment distribution along the (001) crystalline planes of ordered (a) and disordered (b) martensite structures containing Mn atoms located on Mn and Ni positions. Both structures exhibit a ferrimagnetic ground state with distinct configurations of collinear opposite magnetic moments.

are smaller in austenite structure. Whatever the case, the antisite disorder implies in global ferrimagnetic states with small total magnetic moment comparatively to ordered structures. Therefore, these calculation results suggest that the magnetization loss observed in our samples can be explained by the presence of antisite disorder.

3.3. Exchange bias: a phenomenological approach

The origin of the conventional exchange-bias mechanism is indeed the uncompensated AFM spins between antiferromagnet (AF) and ferromagnet (F) at their interface. Since AFM interaction is observed between Mn_{Ni} and Mn_{Mn}, whereas AFM or FM interaction can occur between Mn-Mn pairs depending on Mn-Mn distances [13], it is not surprising the manifestation of the exchange bias in our films.

A simple phenomenological approach [24] for atomically flat AF/F interfaces, disregarding the magnetocrystalline anisotropy, which can be assumed unaffected by the presence of the AF, leads to the following expression for magnetic energy per unit area (in C.G.S.):

$$U = 2J_O \cdot \mathbf{S}_F \cdot \mathbf{S}_{AF} + t_F \cdot M_F \cdot H$$

where J_O is the exchange coupling parameter per unit area at the interface, $\boldsymbol{S}_F$ and $\boldsymbol{S}_{AF}$ refers to the spins of interfacial atoms, M_F is the saturation magnetization of the film, t_F is the thickness, and H is the applied magnetic field. In our case, one can assume a globally ferrimagnetic (Fi) film divided into (antisite) disordered domain-like regions. Typically, compensated/uncompensated interfacial spins can be find along the twin interfaces between variants which coincide with (110) crystallite facets [25]. Atomic terminations at twin planes can form FM/AFM or Fi/AFM interfaces. During the reversal of the film magnetization, the spins of the ordered FM regions rotate coherently, while the spins of the disordered and unbalanced AFM region remain fixed. Therefore, at the switching field of the FM, the pinning energy represented by the first term and the Zeeman energy represented by the second term will balance, resulting in an exchange-bias field H_{EB} given by:

$$H_{EB} = -2J_O \cdot \mathbf{S}_F \cdot \mathbf{S}_{AF} / (t_F \cdot M_F)$$

Thus, the field-shift of hysteresis loop away from zero-field is somehow controlled by strength and sign of J_O which is given by uncompensated spins that predominate at the interfaces. In general, the model depends on the uncompensated AFM interfacial moments, the dimensions of the AFM boundaries, and the presence of interfacial roughness features [24].

A detailed modelling is difficult to implement, but if we assumed the spin values of $S_{AFM} = 2.4\ \mu_B$ and $S_{FM} = 3.3\ \mu_B$ reported in neutron diffraction experiments performed for Mn_2NiGa [13], t_F identical to film thickness of 60 nm, and M_F of the same order of $M_S \sim 1.5\ \mu_B$/f.u., one can estimate J_O values of 0.012 erg/cm^2. We note that the largest exchange bias reversal value is found in stoichiometric Mn_2NiGa with martensite structure, whereas small exchange bias values are found for Ni-rich off-stoichiometric Mn_2NiGa alloys. Exchange bias is an unidirectional anisotropy caused by the spin interactions at magnetic interfaces. Thus, J_O can be expressed as $(N/a^2)J_{EX}$, where N/a^2 is the number of interfacial spins interactions per unit area and *Jex* is the effective magnetic exchange constant. In our case, one expect interactions arising mainly from spin interations between Mn_{Mn} - Mn_{Ni} pairs at interfaces formed by twin planes. By taking $J_{ex} \sim 2.30$ meV for ordered Mn_2NiGa reported by D'Souza and coworkers [7], results that $N/a^2 \sim 2.5 \times 10^{11}$ cm^{-2}, which is about one-thousandth of the surface density of atoms of 2.9×10^{14} cm^2 in the (110) crystalline planes.

By cross-checking DFT calculation results with our simple phenomenological approach, it is expected that when increasing of the Mn_{Ni} antisites some FM/AFM or Fi/AFM interfaces can be formed. Both antisite disorder and Ni content increase can change the FM and AFM interaction imbalance, leading to exchange bias effect. The exchange bias effect for a given alloy composition can be reinforced by decreasing temperature due to significant changes in interatomic distances between Mn and Ni atoms in the martensite structures. Indeed, the presence of Mn_{Ni} antisites can reinforce the AF/F interface interaction in martensite structures, as shown in Figs. 7 and 8, as well as, in austenite structures with contracted lattice parameters, as shown in Figs. 5 and 6. At 10 K, the positive exchange bias observed in alloys with $x = 0$ and 0.2 at low temperature suggest the manifestation of ferrimagnetic/ferromagnetic interfaces, but at 100 K it is apparently simply the temperature above which $H_{EB} = H_C$.

AFM coupling between spins at interfaces between disordered and ordered regions of the film would give rise to positive exchange, if the interface magnetic spins aligned with the applied magnetic field along with the film. The presence of antisite disorder and fluctuations in the Mn-Mn distances probably is behind the intricate behavior of the exchange bias fields as function of the temperature and the stoichiometry, shown in Table 1. The interface between highly textured thin film and substrate is suitable to stabilize metastable domains even others than thermodynamically stable phase. A detailed characterization of local magnetic structure is necessary in order to further understand the magnetic interactions in the films.

4. Conclusions

In summary, we put in evidence that the (110)-textured $Mn_{2-x}Ni_{1+x}Ga$ (x = 0, 0.2, 0.4, and 0.6) films can exhibit the presence of antisite disorder that is usually found in stoichiometric and off-stoichiometric Mn_2NiGa alloys whatever their crystal quality. Such a disorder causes a reduction in the total moment per unit cell and is responsible for engender an intricate exchange bias behavior, including positive exchange bias. Our present results are important to the development of nanodevices based on these magnetic shape memory alloys, where the exchange bias effect plays an important role as a key component in spintronic devices, such as spin-valves and magnetic tunnel junctions.

Acknowledgment

The authors wish to thank CNPq, FINEP, and SISNano for partial financial support and grant of research projects PRONEX/CNPq/Fundação Araucária, CAPES/CNPq/PVE/A083/2013, FAPESP (2009/54082-2 and 2013/07296-2), and the LCPAD (Laboratório Central de Processamento de Alto Desempenho) from Universidade Federal do Paraná by computational support.

References

[1] I. Takeuchi, O.O. Famodu, J.C. Read, M.A. Aronova, K.S. Chang, C. Craciunescu, S.E. Lofland, M. Wuttig, F.C. Wellstood, L. Knauss, A. Orozco, Identification of novel compositions of ferromagnetic shape-memory alloys using composition spreads, Nat. Mater. 2 (2003) 180.
[2] K. Ullakko, J.K. Huang, C. Kantner, R.C. O'Handley, V.V. Kokorin, Large magnetic field induced strains in Ni2MnGa single crystals, Appl. Phys. Lett. 69 (1996) 1966.
[3] G.D. Liu, J.L. Chen, Z.H. Liu, X.F. Dai, G.H. Wu, B. Zhang, X.X. Zhang, Martensitic transformation and shape memory in a ferromagnetic shape memory alloy: Mn2NiGa, Appl. Phys. Lett. 87 (2005) 262504.
[4] W. Cai, J. Zhang, Z.Y. Gao, J.H. Sui, Effect of γ precipitacion martensitic transformation and magnetic properties in aged Mn-Ni-Ga alloys, Appl. Phys. Lett. 92 (2008) 252502.
[5] L. Wollmann, S. Chadov, J. Kubler, C. Felser, Magnetism in tetragonal manganese-rich Heusler compounds, Phys. Rev. B 92 (2015) 064417.
[6] S. Paul, A. Kindu, B. Sanyal, S.J. Ghosh, Anti-site disorder and improved functionality of Mn_2NiX (X = Al, Ga,In, Sn) inverse Heusler alloys, Appl. Phys. 116 (2014) 133903.
[7] S.W. D'Souza, T. Roy, S.R. Barman, A. Chakrabarti, Magnetic interactions and electronic of Ni-Mn-In, J. Phys. Condens. Matter 26 (2014) 506001.
[8] S. Paul, S. Ghosh, First-principles investigations of the electronic structure and properties related to shape-memory behavior in Mn_2NiX (X =Al, Ga, In, Sn) alloys, J. Appl. Phys. 110 (2011) 063523.
[9] G.D. Liu, X.F. Dai, S.Y. Yu, Z.Y. Zhu, J.L. Chen, G.H. Wu, H. Zhu, J.Q. Xiao, Physical and electronic structure and magnetism of Mn_2NiGa: experiment and density-

functional theory calculations, Phys. Rev. B 74 (2006) 054435.
[10] P.J. Brown, T. Kanomata, K. Neumann, K.U. Neumann, B. Ouladdiaf, A. Sheikh, K.R.A. Ziebeck, Atomic and magnetic order in the shape memory alloy Mn2NiGa, J. Phys. Condens. Matter 22 (2010) 506001.
[11] D. Hobbs, J. Hafner, D. Spisak, Understanding the complex metallic element Mn. I. Crystalline and noncollinear magnetic structure of α-Mn, Phys. Rev. B 68 (2003) 014407.
[12] P. Lázpita, J.M. Barandiarán, J. Gutiérrez, J. Feuchtwanger, V.A. Chernenko, M.L. Richard, Magnetic moment and chemical order in off-stoichiometric Ni-Mn-Ga ferromagnetic shape memory alloys, New J. Phys. 13 (2011) 033039.
[13] S. Singh, R. Rawat, S.E. Muthu, S.W. D'Souza, E. Suard, A. Senyshyn, S. Banik, P. Rajput, S. Bhardwaj, A.M. Awasthi, R. Ranjan, S. Arumugam, D.L. Schlagel, T.A. Lograsso, A. Chakrabarti, S.R. Barman, Spin-valve-like magnetoresistance in Mn2NiGa at room temperature, Phys. Rev. Lett. 109 (2012) 246601–246601/5.
[14] D.M. Schaefer, I.T. Neckel, I. Mazzaro, J. Varalda, I.L. Graff, W.H. Schreiner, D.H. Mosca, Martensite transformations in Mn2NiGa thin films grown on GaAs substrates, J. Phys. D. Appl. Phys. 49 (2016) 465002–465002/7.
[15] G. Hollinger, R. Skheyta-Kabbani, M. Gendry, Oxides on GaAs and InAs surfaces: an x-ray-photoelectron-spectroscopy study of reference compounds and thin oxide layers, Phys. Rev. B 49 (1994) 11159.
[16] R.S. Dhaka, S.W. D'Souza, M. Maniraj, A. Chakrabarti, D.L. Schlagel, T.A. Lograsso, S.R. Barman, Photoemission study of the (100) surface of Ni2MnGa and Mn2NiGa ferromagnetic shape memory alloys, Surf. Sci. 603 (2009) 1999–2004.
[17] B.L. Ahuja, G. Ahmed, S. Banik, M. Itou, Y. Sakurai, S. Barman, Compton scattering studies of Mn-rich Ni-Mn-Ga ferrromagnetic shape memory alloys, Phys. Rev. B 79 (2009) 214403.
[18] W.H. Meiklejohn, C.P. Bean, New magnetic anisotropy, Phys. Rev. 105 (3) (1957) 904–913.
[19] K.G. West, D.N.H. Nam, J.W. Lu, N.D. Bassim, Y.N. Picard, R.M. Stroud, S.A. Wolf, Exchange bias in a single phase ferrimagnet, J. Appl. Phys. 107 (2010) 113915.
[20] I. Fita, A. Wisniewski, R. Puzniak, V. Markovich, G. Gorodetsky, Exchange-bias in magnetically compensated ErFe)3 single crystal, Phys. Rev. B 93 (2016) 184432.
[21] The Elk FP-LAPW Code. http://elk.sourceforge.net/.
[22] J.P. Perdew, A. Ruzsinszky, G.I. Csonka, O.A. Vydrov, G.E. Scuseria, L.A. Constantin, X. Zhou, K. Burke, Restoring the density-gradient expasion for exchange in solids and surfaces, Phys. Rev. Lett. 100 (2008) 136406.
[23] K. Momma, F. Izumi, VESTA 3 for three-dimensional visualization of crystal, volumetric and morphology data, J. Appl. Crystallogr. 44 (2011) 1272–1276.
[24] A.E. Berkowitz, K. Takano, Exchange anisotropy – a review, J. Magn. Magn. Mater. 200 (1999) 552.
[25] R. Niemann, et al., Reducing the nucleation barrier in magnetocaloric Heusler alloys by nanoindentation, Adv. Eng. Mater. 14 (2012) 562.